ELSEVIER

Journal of Nuclear Materials 250 (1997) 184–191

journal of nuclear materials

Thermomechanical behavior of actively cooled, brazed divertor components under cyclic high heat flux loads

J.H. You, H. Bolt *, R. Duwe, J. Linke, H. Nickel

Institut für Werkstoffe der Energietechnik, Forschungszentrum Jülich, EURATOM Association, D-52425 Jülich, Germany

Received 25 April 1997; accepted 25 July 1997

Abstract

Actively cooled divertor mock-ups consisting of various low-*Z* armor tiles brazed to refractory metal heat sinks were tested in the electron beam test facility at Jülich. Screening and thermal cycling tests were perfomed on the mock-ups to estimate the overall thermal performance under cyclic high heat flux (HHF) loadings. By detecting the temperature of the armor surface and the braze layer, it was possible to assess the heat removal capability and the accumulation of interfacial damage. Microstructures were investigated to elucidate the degradation of the joints. Finite element analyses are carried out for the simulated HHF test conditions. Temperature fields and thermal stresses are calculated for a typical divertor module. The nature of thermomechanical behavior of the divertor mock-ups under cyclic HHF loadings is discussed. © 1997 Elsevier Science B.V.

1. Introduction

A divertor is an in-vessel component of fusion reactors for power exhaust, impurity control, helium and hydrogen pumping [1]. The particle bombardment will result in an energy transfer in the form of charged particles and neutrals flux onto the divertor plate. During normal operations, the resulting peak heat flux on the divertor plate in the tokamak machine ITER is expected to reach 5 MW/m^2 [2]. Under stationary conditions of the stellarator device Wendelstein 7-X (W7-X), the divertor target plate will be loaded with a maximum local power density of up to 10 MW/m^2 [3]. Under these thermal loading conditions, the critical material requirements for plasma-facing components have to be investigated carefully: physical compatibility with plasma fuels, high thermal conductivity, low tritium inventory, superior high temperature properties and sufficient structural toughness even after irradiations [4,5]. The duplex structures in which plasma-facing armor tiles are brazed to metallic cooling systems have been considered as a candidate design concept for divertor [3,6,7].

Due to the severe temperature gradient and the mismatch in the thermal expansion, significant thermal stresses can be generated in the actively cooled, brazed divertor structures during fusion operations. One of the main types of damage to the divertor joint structures is thermomechanical fatigue, which is a characteristic feature of pulsed operation in tokamak fusion devices [6]. The divertor components in the helias stellarator will also experience thermal cycling when the machine operation is repeated. Thermally induced fatigue is one of the important issues related to long-term lifetime [8,9]. When the material is brittle or the strength of the bond interface is not sufficient, thermal stresses may lead to abrupt failure of the joint structures [10]. Since the available database on interfacial toughness and fatigue behavior of candidate materials is poor, it is necessary to simulate the high heat flux (HHF) fatigue conditions by experiments to assess structural integrity, to characterize the overall thermal response, and to determine the critical heat fluxes.

In investigating the overall thermomechanical performance, it is also of importance to analyze the static thermal stress fields for the load conditions under consideration. When the thermal load varies periodically with time, the corresponding stress changes can result in fatigue

* Corresponding author. Tel.: +49-2461 614 657; fax: +49-2461 613 699.

PII S0022-3115(97)00240-7

damage. In this case, the stress amplitude and the maximum stress level are the critical factors affecting the fatigue lifetime of the structures. In addition, the mean stress value and the mode of the stress change have some influence on fatigue behavior [11,12].

In this work, the thermomechanical performance of actively cooled divertor joint mock-ups is investigated by means of electron beam irradiations. Five different armor materials are tested. Thermal response and microstructural damage under HHF cycling are estimated. Thermal stress fields are calculated employing the finite element method. The analysis is performed for one thermal load cycle of the simulated HHF test condition. The structure-mechanical response of the model component is presented. The time history of the thermal stresses for some critical locations in the module cross section is given.

2. Experiment

2.1. Mock-up description

A set of actively cooled divertor modules with different armor materials was manufactured for the tests. A typical module is shown in Fig. 1. The test mock-up consists of three or four square armor tiles brazed to a metallic heat sink block. The following materials were used:

— armor tiles: Sepcarb N112 (needled 2D CFC), PCC 2S (2D CFC), MFC 1 (1D CFC), RG-Ti (7.5% Ti-doped recrystallized graphite), and SiC 30 (60% SiC–35% graphite–5% Si);

— heat sink block: TZM (Mo–0.5% Ti–0.1% Zr);

— coolant tube connectors: ferritic stainless steel.

The selected materials are presently considered as candidate materials for the divertor elements of the W7-X [3]. They have been also considered as divertor materials for tokamak devices [13–16]. The size of the individual tile is $25 \times 25 \times 10$ mm^3. The heat sink block has a geometry of 25×25 mm^2 in cross section and 100 mm in length. The coolant tube connectors (18 mm in outer diameter, 16 mm in inner diameter) are inserted at both ends. A Cu1Cr braze was used to bond the armor tiles to the TZM heat sink whereas the coolant tube was joined to the TZM body with a Au18Ni braze [17]. The mock-ups were brazed at a brazing temperature of 1100°C under vacuum atmosphere maintaining 1 mm gaps between the tiles. The thickness of the braze layer was about 150 μm. The direction of good thermal conductivity in the tiles is oriented parallel to the incident heat flux.

Table 1
Parameters of the electron beam test facility (JUDITH)

Total power	≤ 60 kW
Power density	≤ 15 GW/m^2
Beam current	≤ 400 mA
Particle energy	≤ 150 keV
Acceleration voltage used	120 kV
Scanning frequency	≤ 100 kHz
Maximum area to be scanned	10×10 cm^2
Coolant flow rate	1.15 l/s

2.2. Test facility

In order to investigate the thermal performance of the divertor mock-ups under HHF loads, the electron beam test facility (JUDITH) at the Research Center Jülich was used. The operational parameters of the facility are listed in Table 1. By means of high frequency beam rastering, the surface of the specimens can be irradiated homogeneously with the well defined loading area. The equipment of the diagnostic system used is as follows: a two-color pyrometer (1000–3500°C); an optical pyrometer (200–1100°C); IR scanner; CCD camera; thermocouples; coolant water calorimetry.

The local surface temperature of the tiles was measured by pyrometers and the whole temperature distribution on the surface was measured by an IR camera. The temperature of the braze layer and the coolant water was detected by thermocouples. There are rastering limits of the electron

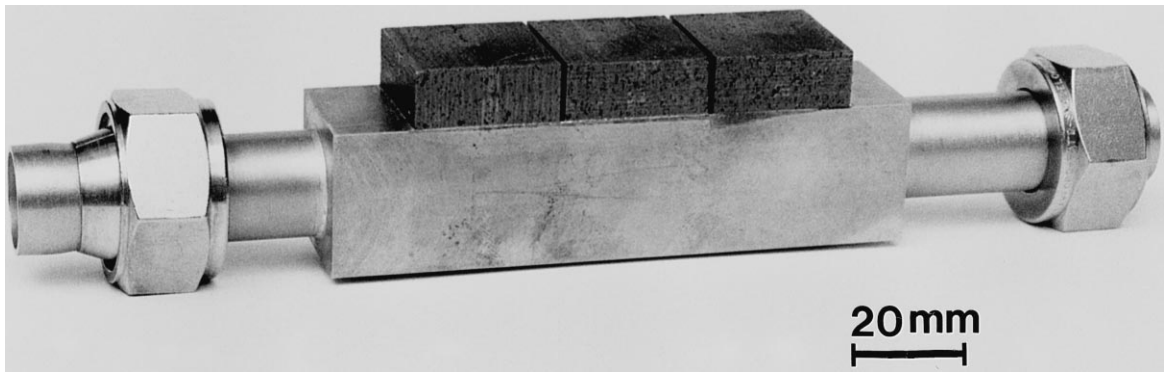

Fig. 1. A brazed, actively cooled divertor module used for the HHF cycling tests.

Table 2
Test conditions for the thermal cycling tests

Armor material	Absorbed power density (MW/m^2)	Number of cycles
Sepcarb N112 (needled 2D CFC) (Societé Européenne de Propulsion)[a]	12	30
	10.5	50
PCC 2S (2D CFC) (Hitachi)[a]	10.5	30
MFC 1 (1D CFC) (Mitsubishi)[a]	7	30
RG-Ti (Ti-doped graphite) (Efremov Institute)[a]	10.5	[b]
SiC 30 (SiC with 35% C) (Schunk Kohlenstoff)[a]	7	[b]

[a] Manufacturer.
[b] The module joints were debonded during the second shot.

beam on the armor surface since the high energy beam raster should fall short of the ends of the armor. The effective loading area becomes a little bit smaller than the actual tile surface. This may lead to different power density values along the heat flow direction. However, the high thermal diffusion would homogenize the horizontal temperature field except for the surface region. Thus, the rastering limit has no influence on the thermomechanical behavior of the bond interface. In this work, the nominal heat flux is calculated based on the actual surface area whereas the net heat flux absorbed is determined by the coolant water calorimetry.

2.3. Pre-inspection of the mock-up joints

Before the main tests were carried out, the whole divertor mock-ups were subjected to low heat fluxes to inspect the quality of the bond interface. The temperature distribution on the whole surface was displayed in color shading by the use of IR thermography. Brazing defects, where the thermal contact is poor, can be detected by the local temperature elevation. The protection tiles with an intact bond interface were selected and used for further testing.

2.4. Screening tests

Screening tests were performed to estimate the limit of tolerable thermal loads. The incident power levels were increased stepwise from shot to shot. The pulse duration was 30 s. The absorbed net power density deposited on the tiles is lower than the nominal power density due to the reflection of electrons. Since the heat flux to be removed by the coolant during steady-state conditions is balanced by the heat flux to be deposited on the tile surface, the net energy flux can be calibrated by measuring the removed heat. The power density was increased until considerable thermal erosion occurred or the joint failed due to thermal shock. The tests were terminated to avoid extensive sublimation of carbon although the brazed joints presumably could have survived higher power levels.

2.5. Thermal cycling tests

To assess the fatigue behavior of the mock-ups under pulsed thermal loads, thermal cycling tests were conducted. The experimental parameters are summarized in Table 2. The duration of electron beam irradiation for all shots was kept constant at 30 s. The period of each thermal pulse including the cooling phase was about one minute. Thermal equilibrium was reached after 20 s. The maximum surface temperature of the tiles in steady-state conditions and its change during cyclic loading were measured. The propagation of interfacial defects was traced by IR thermography for each beam shot.

3. Numerical analysis

3.1. Model

The thermal and elastoplastic stress analyses were performed for the divertor modules in HHF tests using the finite element (FE) code ABAQUS [18]. Only half of the geometry was considered due to symmetry. The two-dimensional finite element mesh includes 296 eight-noded quadrilateral elements and 1059 node points. For stress analysis, generalized plane strain elements were used to consider the out-of-plane strain. The thin, ductile braze layer was neglected in the model. The material combinations selected for the analysis are identical to those of the divertor modules tested for the HHF simulation. The anisotropy and temperature dependence of the material properties were taken into account. The time-dependent effects were not included. It was assumed that all five armor materials behave elastically. Elasto-plastic behavior was assumed for the metallic cooling body. The applied plasticity of the metals was based on stepwise linear stress–strain relations and the isotropic hardening law.

3.2. Thermal analysis

Thermal analysis precedes the stress analysis to produce the input temperature data for the following stress calculations. The surface of the armor tiles was subjected

to a uniform heat flux of 10.5 MW/m^2 for 30 s. The coolant water temperature was 20°C at a flow velocity of 6 m/s. The coolant heat transfer coefficient was computed as a function of the cooling tube wall temperature assuming two-phase heat transfer. Cooling by radiative emission was considered. A cooling down phase of 20 s followed the thermal load pulse.

3.3. Stress analysis

The brazing simulation was carried out prior to the HHF loading step to take the residual stresses at room temperature into account. It was assumed that the temperature distribution was kept homogeneous during the cooling of brazing process. The stress-free reference temperature was taken as 1070°C, which was the solidus temperature of the braze metal. The subsequent secondary stress fields caused by HHF thermal loads is superposed onto the residual stress. The stress evolution corresponding to the single load cycle of 50 s was calculated. The internal pressure of the coolant tube was neglected in order to observe the purely thermally induced stress state. In the analysis, the cooling tube connector was not considered since it was inserted just in the edge part of the coolant channel.

4. Results and discussion

4.1. Experimental results

The thermophysical properties of materials used for the divertor mock-ups are presented in Figs. 2 and 3 [19–25].

Fig. 4 shows the thermal response of a divertor mock-up (Sepcarb N112/TZM joint) under an absorbed thermal power density of 10.5 MW/m^2 with a pulse duration of 30 s. The temperature evolution of the armor surface measured by the pyrometer is compared to the numerical result obtained from the finite element analysis. Since

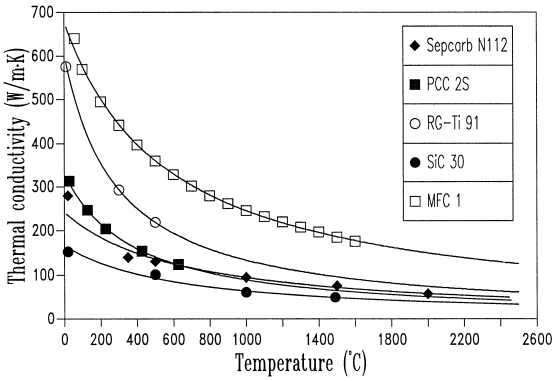

Fig. 2. Thermal conductivity of the divertor materials for the orientation parallel to fiber plane [14–20].

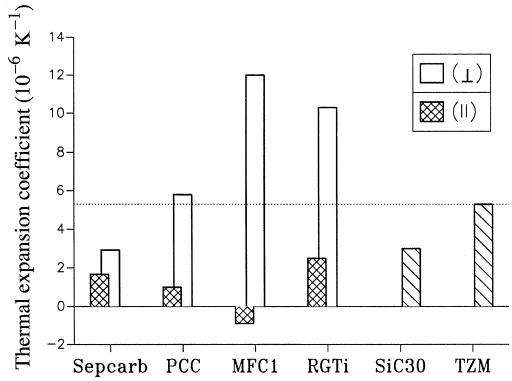

Fig. 3. Linear thermal expansion coefficient of the divertor materials at room temperature [14–20].

some of the incident electrons are reflected, an electric power density of 13 MW/m^2 was needed to generate the net thermal power density of 10.5 MW/m^2 on the divertor armor surfaces. The rise time to reach full power and the time to zero power was one second. Steady-state conditions were achieved after 20 s by equilibrium between the input heat flux and the heat removed via the coolant. The results show a good agreement in the steady state. In the transient phase, there is a slight difference. It can be seen that the surface region experiences a temperature change of more than 2000°C within 10 s.

The steady-state surface temperatures of the five divertor mock-ups under HHF simulation conditions are given in Fig. 5. The experimentally measured values as well as the numerically calculated results are presented. The SiC30/TZM mock-up was tested for a lower power density of 7 MW/m^2 because it could not survive under higher power density.

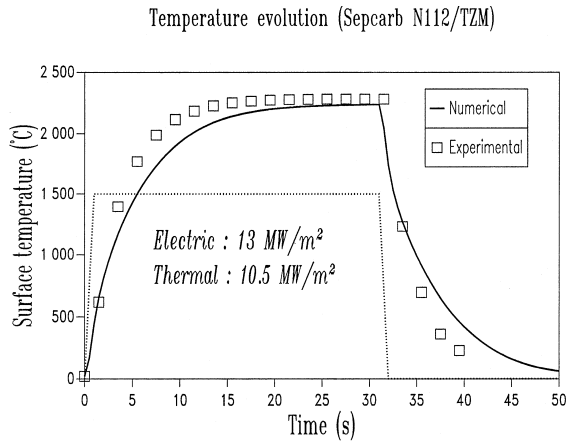

Fig. 4. Thermal response of the divertor mock-up, Sepcarb N112/TZM joint (power density: 10.5 MW/m^2, pulse duration: 30 s).

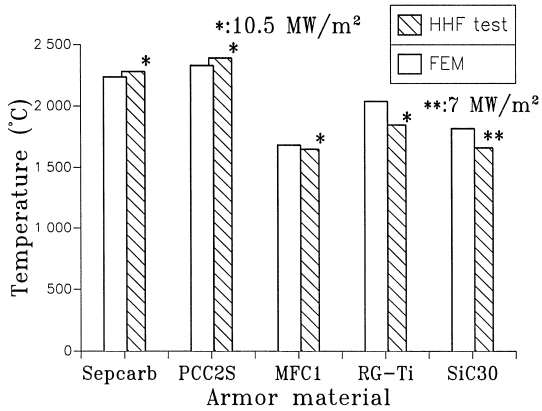

Fig. 5. Surface temperature of the divertor mock-ups in the steady state of the HHF loading (power density: 10.5 MW/m^2 or 7 MW/m^2, pulse duration: 30 s).

The thermal performance of the mock-ups measured in the screening tests is given in Fig. 6. Within the range of applied heat flux, which varies from 7.2 MW/m^2 to 12 MW/m^2, the temperature increases proportionally with the power density. The sequence of the surface temperature values shows a reciprocal relationship with the thermal conductivities in Fig. 2. This can be clearly understood since the surface temperature depends directly on the ability to transfer the deposited heat to the metallic cooling body. When the thermal conductivity of the metallic body is much lower than that of the armor material, as is the case for TZM, the thermal flow will be retarded at the interface. In this case, the armor tile with high thermal conductivity undergoes a thermal equilibration where the interface temperature is increased. This effect is demonstrated in Fig. 6(b), where the interface temperature value increases with increasing thermal conductivity. The braze interlayer in the mock-up with the MFC1 armor was melted during the 10.5 and 12 MW/m^2 shots.

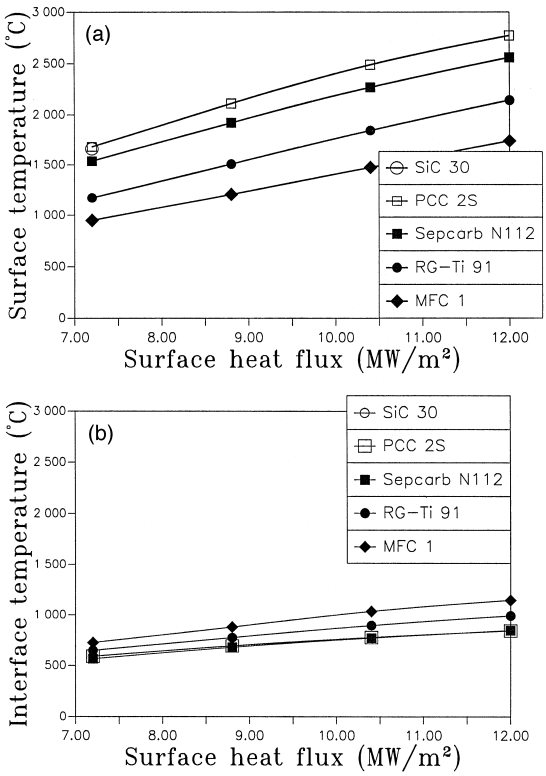

Fig. 6. Thermal performance of the divertor mock-ups for various levels of power density, the temperatures were measured in the steady state; (a) tile surface temperature, (b) bond interface temperature.

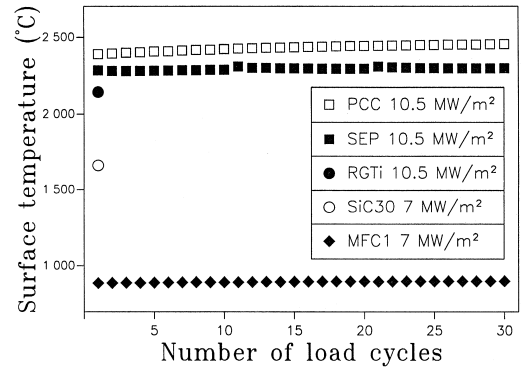

Fig. 7. Fatigue behavior of the divertor mock-ups under cyclic HHF loads.

Fig. 7 shows the fatigue behavior of the mock-ups under cyclic HHF loads. The individual points in the plot represent the temperature of the tile surface during the steady state in each thermal cycle. The mock-ups with the SiC30 and RG-Ti armors could only survive the first shot even under reduced power density (7 MW/m^2). The interface of these mock-ups showed abrupt fracture during the second shot. The mock-ups armored with CFC materials showed relatively good fatigue resistance.

Fig. 8 shows the cross-section of the debonded divertor mock-up. The divertor module was cut by the water jet technique. The interface of the mock-ups armored with ceramic and graphite tiles was debonded by brittle fracture. On the contrary, none of the mock-up cross sections consisting of the CFC/TZM joint show any macroscopically observable fatigue damage. The bond interface in the CFC/TZM divertor joints remained sufficiently intact and produced only minute microscopic flaws after the tests.

4.2. Computational results

In the following, the structure-mechanical response of the divertor test mock-ups is discussed. The analysis was carried out using the finite element method. The temperature cycle in Fig. 4 coupled with the given input HHF

Fig. 8. Cross-section of the debonded divertor mock-up tested in the HHF cycling simulation (SiC 30-to-TZM module: 7 MW/m^2, 2 cycles).

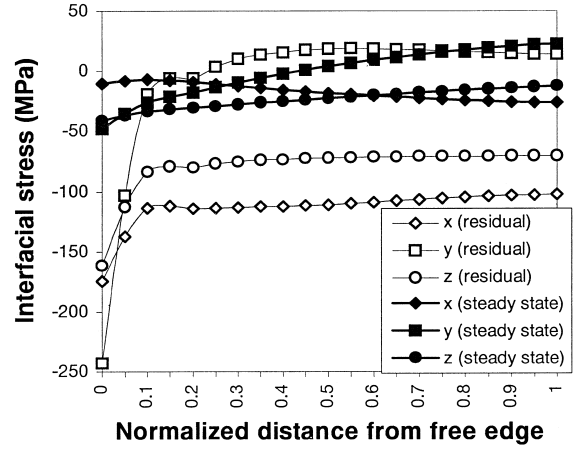

Fig. 10. Thermal stress along the bond interface of the CFC armor tile (Sepcarb N112/TZM joint: 10.5 MW/m^2, 30 s).

pulse was taken as the reference thermal loading history for the stress calculation. As a representative case, the result for the Sepcarb N112/TZM joint is presented in detail.

Fig. 9 shows the deformed structures of the mock-up cross section with a displacement magnification of twenty times. The divertor mock-ups consisting of the other material combinations showed the same feature in the deformed structure except for the MFC1/TMZ joint. The MFC1 tile shrinks more than the TZM body in the residual stress state due to its high CTE (coefficient of thermal expansion) value (cf. Fig. 3).

The interfacial stresses along the bond interface of the CFC side are plotted in Fig. 10. The results are given in three stress components both for the residual stress state and for the steady state of the HHF loading. The stress values are overestimated compared to the actual case since the ductile braze layer is neglected in the stress analysis. It can be seen that the interfacial stresses are considerably relieved during the HHF loading. Significant stress concentration occurs near the free surface edge. It has been extensively reported that the stress concentration occurs in the region near the free surface edge of the bond interface sometimes showing singularities [26]. This is due to the complicated deformation of the free surface near the material interface, where the assumption of the beam theory is

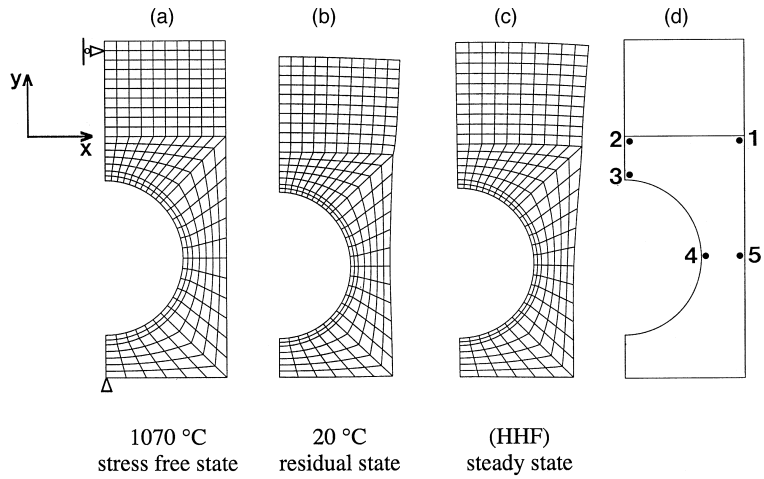

Fig. 9. Deformed structure of the divertor cross section (Sepcarb N112/TZM joint). (a) Stress-free state (at brazing temperature), (b) residual stress state (at room temperature), (c) steady state in the HHF loading (10.5 MW/m^2, 30 s), (d) points of stress history analysis in Fig. 11.

not valid [27]. In general, the result of the structural finite element analysis including field discontinuities is affected by the degree of mesh refinement. The maximum magnitude of the stress components would increase when the FE mesh is more refined [28]. In this work, however, the stress singularity will not be treated for the simplicity of the numerical analysis. In the present FE model, the stress values near the free surface edge of the bond interface are averaged and interpolated in each element. The stress singularity can exist only in an ideally elastic continuum. Due to the strain energy dissipation caused by a micro-flaw formation in the composite structure or by a small scale yielding, the real stress gradient in the singular field would be blunted. On the other hand, the bulk stress will not be influenced significantly. Since all the singular stress components are in compressive state, the intensified stress fields will not lead to an abrupt fracture.

The time history of the von Mises equivalent stress is plotted in Fig. 11 for some selected positions in the TZM heat sink. The locations considered are shown in Fig. 9. At the residual state, the stress distribution in the metallic cooling substrate is relatively homogeneous. The maximum equivalent stress in the residual state is below 300 MPa. In the steady state of the HHF loading, the cooling liner wall experiences much higher thermal stress as well as larger stress range than the other locations. The level of the equivalent stresses distributed in the TZM cooling body remained under the elastic limit during the whole loading cycle except for the local liner wall near position 3. In spite of the as high equivalent stress values as at position 3, the liner wall near the position 4 does not exceed the 0.2% offset yield limit due to the lower temperature in that region. The stress at position 3 increases again in the cooling phase instead it recovers its residual stress state. This is caused by a plastic deformation in this region. When the elastic media surrounding the yielded zone tends to be undeformed during the cooling phase, it exerts a traction on the plastically deformed zone resulting in stresses. The calculated equivalent plastic strain at position 3 is 0.275%. If the FE model had a very fine discretization in the region near the free edge of the bond line, the equivalent stress values would exceed the yield strength of TZM showing blunted stress concentration in that region. The interface of TZM (points 1 and 2) shows a doubled cycling of equivalent stress in the HHF cycle. It might be due to the high temperature gradient induced by the HHF pulse load which leads to a characteristic thermal deformation behavior of the given structure. Considering the mechanical strength of TZM, the thermomechanical loading in the metallic cooling substrate seems to be less serious than that of the armor tiles.

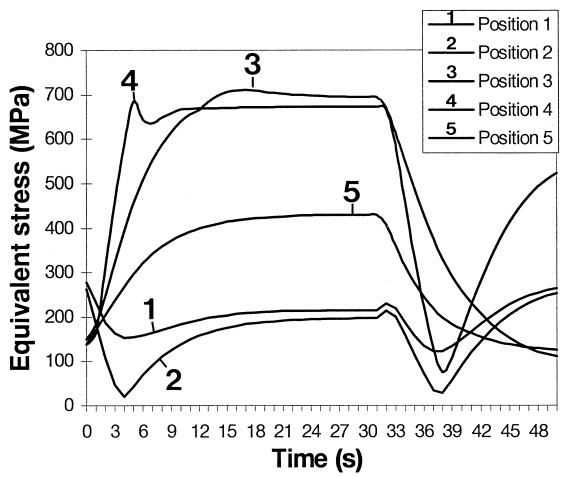

Fig. 11. Time history of the equivalent stress in the TZM body during the HHF loading cycle (Sepcarb N112/TZM joint: 10.5 MW/m^2, 30 s).

5. Summary

To simulate the cyclic HHF operations of the divertor components, actively cooled, joint mock-ups were tested under cyclic electron beam irradiations. Five different bond combinations were used in which nonmetallic armor tiles were brazed onto the TZM heat sink.

For the reference power density of 10.5 MW/m^2, thermal equilibrium was achieved within 20 s. The experimental results for the thermal response of the divertor mock-ups showed good agreement with the numerical analysis. The test mock-up with the MFC1/TZM joint showed an excellent heat removal ability. In the screening tests, the temperatures increased linearly with the input power density ranging from 7 MW/m^2 to 12 MW/m^2. The mock-ups armored with CFC tiles showed a good fatigue resistance up to 30 cycles and their thermal performance was stable. On the contrary, the mock-ups with graphite or ceramic tiles could only survive a single shot resulting in an abrupt fracture of the bond interface.

The finite element method was employed to calculate the temperature and stress fields of the test mock-ups. The divertor mock-up with the Sepcarb N112/TZM joint was analyzed in detail. In the steady state, a temperature difference of 1200°C developed within the armor tile thickness. The interfacial stresses were considerably relieved during the thermal loading. The free edge region of the bond interface was the critical location in the residual stress state whereas the cooling liner wall in the TZM substrate was most severely stressed by the HHF thermal loading. The upper part of the cooling liner wall yielded during the HHF loading. In the free edge region of the CFC interface, significant stress intensification occurred. Due to the compressive state, the stress intensification did not lead to an abrupt fracture.

References

[1] K.J. Dietz, S. Chiocchio, A. Antipenkov, G. Federici, G. Janeschitz, E. Martin, R.R. Parker, R. Tivey, Fus. Eng. Des. 27 (1995) 96.

[2] ITER Joint Central Team, J. Nucl. Mater. 212–215 (1994) 3.

[3] H. Greuner, W. Bitter, F. Kerl, J. Kisslinger, H. Renner, Fusion Technol. 1 (1994) 323.

[4] P. Schiller, J. Nihoul, J. Nucl. Mater. 155–157 (1988) 41.

[5] R.F. Mattas, D.L. Smith, C.H. Wu, T. Kuroda, G. Shatalov, J. Nucl. Mater. 191–194 (1992) 139.

[6] E. Zolti, J. Nucl. Mater. 155–157 (1988) 386.

[7] G. Federici, R. Matera, S. Chiocchio, J. Dietz, G. Janeschitz, D. Driemeyer, J. Haines, M.S. Tillack, M. Ulrickson, Fus. Eng. Des. 28 (1995) 34.

[8] M. Araki, M. Akiba, M. Dairaku, K. Iida, H. Ise, M. Seki, S. Suzuki, K. Yokoyama, J. Nucl. Sci. Technol. 29 (9) (1992) 901.

[9] S. Deschka, A. Cardella, J. Linke, M. Lochter, H. Nickel, J. Nucl. Mater. 203 (1993) 67.

[10] Y. Yoshino, H. Ohtsu, T. Shibata, J. Am. Ceram. Soc. 75 (1992) 3353.

[11] T.V. Duggan, J. Byrne, Fatigue as a Design Criterion, Macmillan, London, 1977.

[12] J.A. Bannantine, J.J. Comer, J.L. Handrock, Fundamentals of Metal Fatigue Analysis, Prentice Hall, NJ, 1990.

[13] M. Akiba, H. Bolt, R. Watson, G. Kneringer, J. Linke, Fus. Eng. Des. 16 (1991) 111.

[14] P. Schiller, K. Ehrlich, J. Nihoul, J. Nucl. Mater. 179–181 (1991) 13.

[15] S. Deschka, A. Cardella, J. Linke, M. Lochter, H. Nickel, J. Nucl. Mater. 203 (1993) 67.

[16] H. Horiike, Fus. Eng. Des. 16 (1991) 275.

[17] R. Lison, Z. Mirski, J. Linke, Proc. Hart- und Hochtemperaturlöten und Diffusionsschweißen 92, DVS-Berichte Band 148, Deutscher Verband für Schweißtechnik, Aachen, 1992, pp. 289–294.

[18] ABAQUS Users Manual 5.4, Hibbit, Karlson and Sorenson, Providence, RI, 1994.

[19] I. Smid, M. Akiba, M. Araki, S. Suzuki, K. Satoh, Material and Design Considerations for the Carbon Armored ITER Divertor, Japan Atomic Energy Research Institute, JAERI-M 93-149, 1993.

[20] E. Zolti, Material Data for Predesign Analysis of In Vessel Components, ITER Internal Report ITER-IN-N/I/3300/5/A, 1990.

[21] Sepcarb N112: A general presentation, Sep Documentation, MC-33395/91 LF/mmd, Societé Européenne de Propulsion, 1991.

[22] JAERI JT-60 Team, Japan Atomic Energy Research Institute, JAERI-M 90-119, 1990.

[23] T.A. Burtseva, O.K. Chugunov, E.F. Dovguchits, I.V. Mazul, Shibkov, V.A. Sokolov, M.I. Persin, P.A. Platonov, in: B. Krahl-Urban, D. Clemens (Eds.), Carbon Materials — Binary Materials for Plasma Facing Components, Proc. 6th Int. Workshop on Carbon Materials, Jülich, Germany, 1993, p. 43.

[24] Datenblatt: Werkstoff-SiC30, wfr 9/91, Schunk Kohlenstofftechnik GmbH, 1991.

[25] L. Binkele, personal communication (1993).

[26] J.P. Blancard, N.M. Ghoniem, Trans. ASME J. Appl. Mech. 56 (1989) 756.

[27] R. Viola, E.B. Deksnis, Geometry free of singularities for fusion duplex components, JET-P (94) 54, JET Joint Undertaking, November, 1994.

[28] J.D. Whitcomb, I.S. Raju, J.G. Goree, Comput. Struct. 15 (1) (1982) 23.